Nanoindentation shape effect: experiments, simulations and modelling

2007 J. Phys.: Condens. Matter 19 395002

(http://iopscience.iop.org/0953-8984/19/39/395002)

IOP PUBLISHING JOURNAL OF PHYSICS: CONDENSED MATTER

J. Phys.: Condens. Matter **19** (2007) 395002 (12pp) doi:10.1088/0953-8984/19/39/395002

Nanoindentation shape effect: experiments, simulations and modelling

L Calabri[1], N Pugno[2], A Rota[1], D Marchetto[1,3] and S Valeri[1,3]

[1] CNR-INFM—National Research Center on nanoStructures and bioSystems at Surfaces (S3), Via Campi 213/a, 41100 Modena, Italy
[2] Department of Structural Engineering, Politecnico di Torino, Corso Duca degli Abruzzi 24, 10129 Torino, Italy
[3] Department of Physics, University of Modena and Reggio Emilia, via Campi 213/a, 41100 Modena, Italy

E-mail: calabri.lorenzo@unimore.it

Received 13 February 2007, in final form 20 March 2007
Published 30 August 2007
Online at stacks.iop.org/JPhysCM/19/395002

Abstract

AFM nanoindentation is nowadays commonly used for the study of mechanical properties of materials at the nanoscale. The investigation of surface hardness of a material using AFM means that the probe has to be able to indent the surface, but also to image it. Usually standard indenters are not sharp enough to obtain high-resolution images, but on the other hand measuring the hardness behaviour of a material with a non-standard sharp indenter gives only comparative results affected by a significant deviation from the commonly used hardness scales.

In this paper we try to understand how the shape of the indenter affects the hardness measurement, in order to find a relationship between the measured hardness of a material and the corner angle of a pyramidal indenter. To achieve this we performed a full experimental campaign, indenting the same material with three focused ion beam (FIB) nanofabricated probes with a highly altered corner angle. We then compared the results obtained experimentally with those obtained by numerical simulations, using the finite element method (FEM), and by theoretical models, using a general scaling law for nanoindentation available for indenters with a variable size and shape.

The comparison between these three approaches (experimental, numerical and theoretical approaches) reveals a good agreement and allowed us to find a theoretical relationship which links the measured hardness value with the shape of the indenter.

The same theoretical approach has also been used to fit the hardness experimental results considering the indentation size effect. In this case we compare the measured data, changing the applied load.

(Some figures in this article are in colour only in the electronic version)

1. Introduction

Over the last few decades, nanoindentation techniques have been explored by many researchers all over the world [1–11] and extensively used to investigate different mechanical properties, such as hardness modulus, Young's modulus and properties of thin films and coatings.

The idea of nanoindentation arose from the necessity to measure the mechanical properties of very small volumes of materials. In principle, if a very sharp tip is used the volume of material that is tested can be made arbitrarily small, but in this case is very difficult to determine the indentation area. To solve this problem several depth sensing indentation (DSI) methods were developed [1, 4, 5].

In general, the hardness is defined as the ratio between the maximum applied load (P_{max}) and the projected area of the indentation impression (A_c). In particular, most of the recent studies concerning hardness measurement are based on the analysis of the load–displacement curves resulting from the nanoindentation test using the Oliver and Pharr (OP) method [3–5].

The OP method allows hardness measurement without imaging the indentation impression, since it establishes a relationship between the projected area of the indentation impression, the maximum depth of indentation (h_{max}) and the initial unloading stiffness (S), where h_{max} and S are both measurable from the load–displacement curve. In this way it is possible to obtain the mechanical properties without having to see the indentations.

Hardness is an intrinsic property of materials and in the past all researchers assumed that it can be treated as a constant. In contrast, in recent years many studies have demonstrated that there is an indentation size effect (ISE) in the hardness measurement and in particular that it varies with the applied load [2].

In the present paper we address the indentation shape effect (IShE), which is connected to the shape of the indenter (not to the indentation depth). Obviously in changing the shape of the indenter (and in particular the tip corner angle) the behaviour of the material penetration process changes. In this paper we try to understand how this affects the measured hardness value in terms of pressure (ratio between the maximum applied load and the projected area of the indentation).

In order to gain a basic knowledge of the IShE, nanoindentation was performed on a soft photoresist material (*Microposit s1813 photoresists*) using FIB nanofabricated silicon probes with different tip corner angles. The resultant load–displacement curves were analysed using the OP method (even if in this case the pile-up effect is not negligible and the OP method rather overestimates the hardness values). Then the effect of the indenter shape on the determination of hardness modulus was examined.

We address this kind of problem because to investigate the surface hardness at the nanoscale it is useful to perform nanoindentation and subsequently image the corresponding surface modification using an AFM. Usually standard indenters are not sharp enough for imaging with good resolution (the sharpest standard indenter is the cube corner probe, with a tip angle of 90°). On the other hand, measuring the hardness behaviour of a material with a non-standard sharp indenter gives only comparative results, affected by a significant deviation from the commonly used hardness scales.

For this reason we approach here this kind of problem, in order to find a relationship between the hardness of a material and the shape of the indenter and to define a new method to have a precise measurement of material hardness and simultaneous high-resolution imaging. With this kind of approach it will be easy to measure the hardness both with the DSI method, using the load–displacement curves, and with the imaging method, measuring the contact area directly on the indentation impression.

To avoid the OP overestimation of results connected to the presence of a non-negligible pile-up, we also evaluated the hardness with this second technique, measuring the contact area

Table 1. Mechanical properties of the specimen material (photoresist).

Mechanical property	Reference value
Microhardness	∼200 MPa
Ultimate tensile strength	51.2 MPa
Yield tensile strength	43 MPa
Elongation at break	0.6%
Young's modulus	8 GPa
Poisson's ratio	0.33

directly. The results are definitely closer to the actual hardness of the material and also to the numerical data, as reported in section 5.

During the experiments several non-ideal conditions (such as pile-up formation, x-movement of the AFM cantilever and non-linear contact area, effects that, at the nanoscale, depend on the tip curvature) may affect the results and make the comparison with the numerical and theoretical analysis absolutely non-trivial.

2. Experimental configuration

The set of indenters used in this work is commercial silicon AFM tips; in particular, we used *MPP-11100-Tap300 Metrology Probes* from *Veeco*®. We decided to use this kind of indenter because they are a good compromise between cost and mechanical properties. Other solutions are in fact too expensive (i.e. reshaping of diamond tips) or have unknown mechanical properties (i.e. ultra-hard coated AFM tips with the substrate deformable during indentation).

The present solution allows an easy approach to the problem. The commercial silicon AFM tips are easy to find, cheap and reshapable with the FIB nanofabrication process. This kind of tip is silicon made and consequently could not provide a high mechanical profile in terms of hardness and non-deformability. For this reason we decided to use them to indent a soft substrate in order to keep a high ratio between the hardness of the indenter and the hardness of the sample. In this way the silicon tips, even if provided with a poor hardness value, will be basically non-deformable when pressed on the selected soft material. The substrate we used is a photoresist material, namely *Microposit s1813 photoresist* by *Shipley*®. It is a *positive* photoresist based on a *NOVOLAC* polymer. Its mechanical properties are reported in table 1. This material is ideal for this kind of study, because it is very soft, thus easy to indent with a silicon tip, and at the same time it is very flat, allowing an accurate measurement of the indentation projected area.

2.1. FIB nanofabrication

The pristine geometry of the probe tip is a quadratic pyramid (figures 1(a) and (b)). As reported in the Veeco® probe catalogue the characteristic geometry of the tip is listed in the inset table of figure 1(b).

In this work, in order to obtain a set of indenters with a variable corner angle, we functionalized these pristine probes with the aim of transforming them into a triangular pyramid (as the nanoindenters usually are). There are several different approaches to perform this kind of customization, but we decided to carry it out by nanofabricating the tips with a FIB apparatus. The FIB system is a dual-beam machine (*FEI StrataTM DB 235*) combining a high-resolution FIB column equipped with a Ga liquid metal ion source (LMIS) and an SEM column equipped

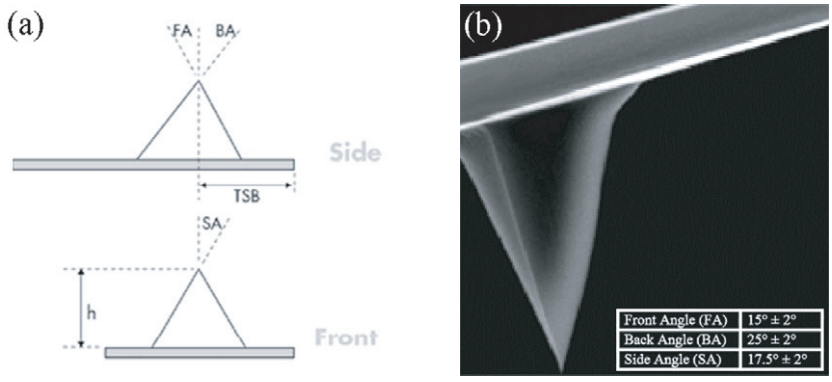

Figure 1. (a) Schematic diagram of the tip geometry (from the Veeco® probe catalogue); (b) image of the pristine probe (from the Veeco® probe catalogue).

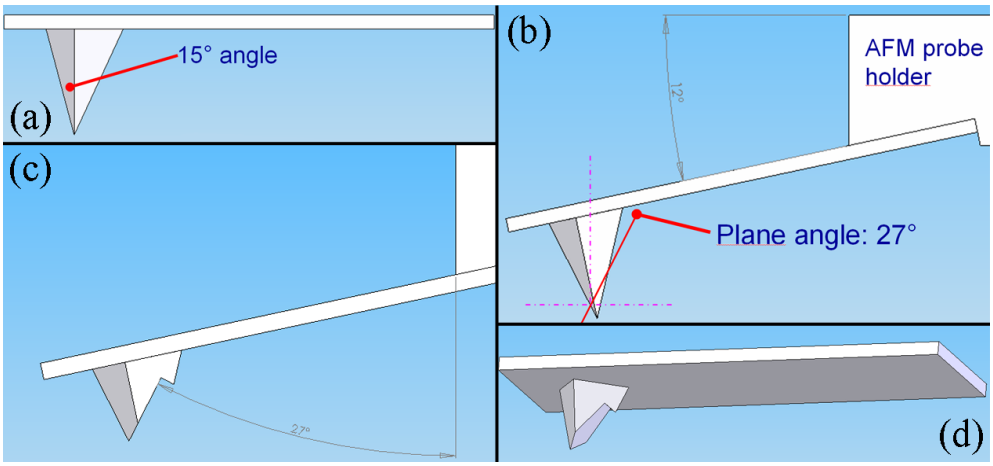

Figure 2. (a) Probe pristine geometry; (b) position of the cutting plane; (c) tip profile after the reshape phase; (d) 3D design of the customized probe.

with a Schottky field emission gun (SFEG) electron source. FIB offers the ability to design, sculpt or pattern nano- and microstructures on different materials with spatial resolution down to 20 nm.

By means of the FIB machine we proceeded to cut the pristine probe with a plane positioned with proper different orientations. In this way we utilized two pristine faces of the original tip and we just created the third face. In figure 2 is reported the reshaping procedure step by step: figure 2(a) is the pristine geometry; figure 2(b) is the position of the cutting plane (the plane is perpendicular to the image and the red line is its trace on the page); figure 2(c) is the tip shape after the reshape phase; figure 2(d) is the 3D design of the customized probe.

With this procedure we realized three different indenters. In figure 3 the SEM images of the three probes obtained by FIB nanofabrication are reported. The angles of the cutting plane are chosen in order to obtain a new tip which is able to approach the sample during the indentation procedure perpendicular to the sample surface. To achieve this we always took into account the 12° angle of the AFM probe holder (figure 2(b)). The second probe is obtained

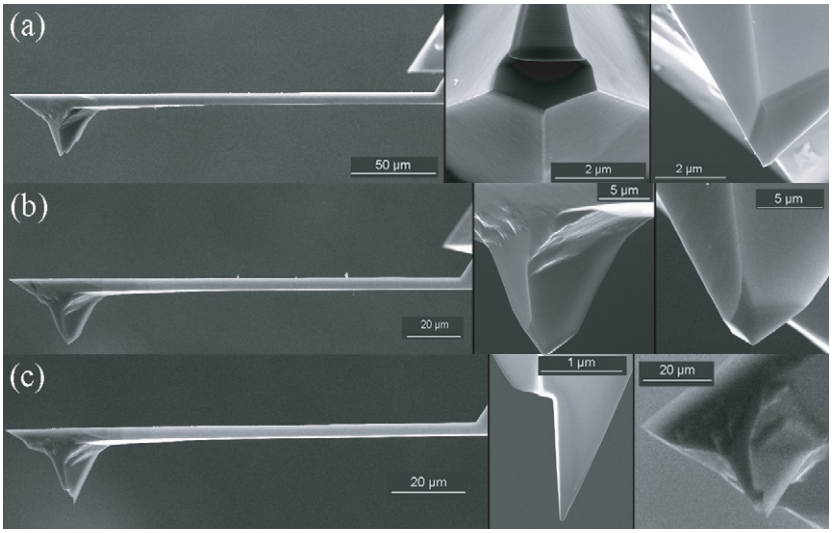

Figure 3. SEM images of the customized probes: (a) indenter n°1—equivalent corner angle of 62°; (b) indenter n°2—equivalent corner angle of 97°; (c) indenter n°3—equivalent corner angle of 25°.

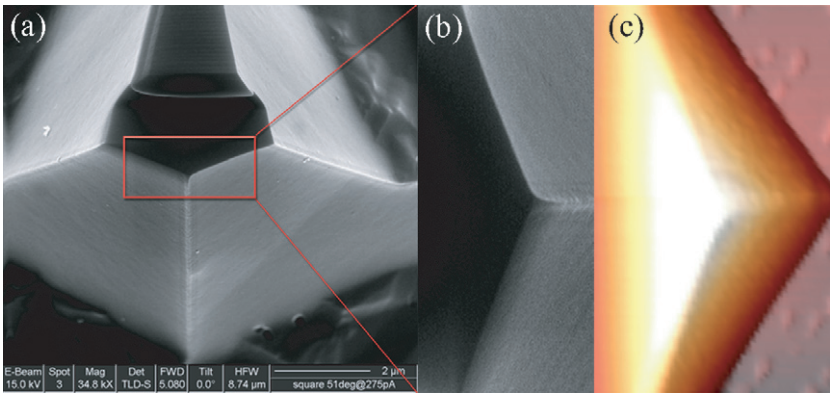

Figure 4. (a), (b) SEM images of the customized probe n°1; (c) AFM image on the calibration grid of the customized probe n°1.

cutting the tip with three different planes (there was no chance in fact to utilize any pristine face of the original probe) and the shape was completely recreated (figure 3(b)).

In figure 4 one can see the final shape of customized probe n°1, observed with an SEM microscope (figures 4(a) and (b)) and also with an AFM (figure 4(c)) using a calibration grid composed of an array of sharp tips (test grating *TGT1–NT-MDT*®).

The final shape of the indenters is a triangular pyramid with a customized geometry. To codify the new geometry of the nanofabricated probes we decided to refer to the *equivalent corner angle.*

The equivalent corner angle of a triangular pyramid is defined as the corner angle of a conical indenter with the same area function. Using this kind of codification we obtained for the three functionalized indenters the equivalent corner angles listed in table 2.

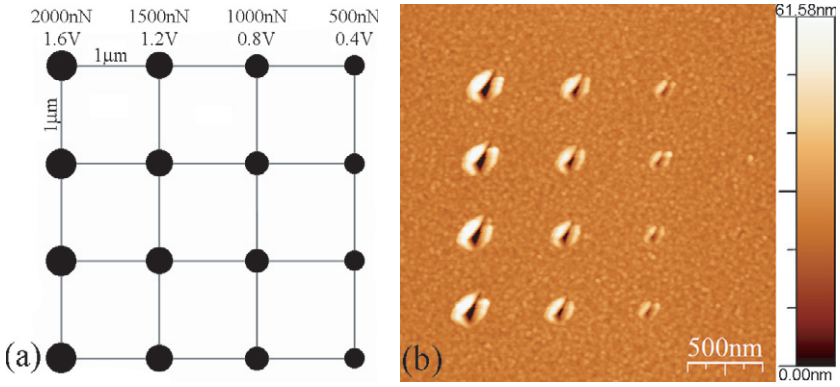

Figure 5. (a) Schematic diagram of the indentation matrix; (b) AFM image of the indentation matrix.

Table 2. Equivalent corner angles of the nanofabricated probes.

Indenter	Equivalent corner angle (deg)
Probe n°1	62
Probe n°2	97
Probe n°3	25

2.2. Experimental nanoindentation set-up

The whole experimental campaign is performed using AFM nanoindentation. The instrument we used is a *Digital Instruments EnviroScope Atomic Force Microscope* by *Veeco*®. This instrument allowed us to indent the sample and image it right after the indentation.

The experimental phase consists of five matrices of indentations performed for each probe at exactly the same conditions. Each matrix (figure 5(a)) consists of 16 indentations performed at different loads on a row and repeated column by column. The indentations reported in figure 5(b) reveal a clear pile-up. This phenomenon is connected to the material, which is really soft, and also to the geometry of the tip (decreasing the corner angle of the tip increases the plastic deformation of the material and thus its pile-up).

The loads applied on the sample vary from 0.4 to 1.6 V in terms of photodetector voltage. Thus, considering the cantilever spring constant and the deflection sensitivity, we obtain a maximum load for the three indenters of about 2000 nN.

As long as the probes we used are commercial AFM tapping probes, they are not calibrated in terms of elastic spring constant. Thus, to calibrate them, we used the classical Sader approach to the problem [12, 13]. We measured by SEM the exact geometry of the cantilever and by AFM the proper frequency of vibration in air.

The deflection sensitivity is then calibrated using the load–displacement curves and it corresponds to the slope of the force plot in the contact region. The deflection sensitivity is the factor which allows us to convert the cantilever deflection from volts to nanometres.

The results in terms of elastic spring constant and deflection sensitivity for the three probes are reported in table 3.

3. Numerical model

The finite element method is here used to simulate the indentation process in order to find a numerical correlation between the hardness value and the shape of the indenter. To create the

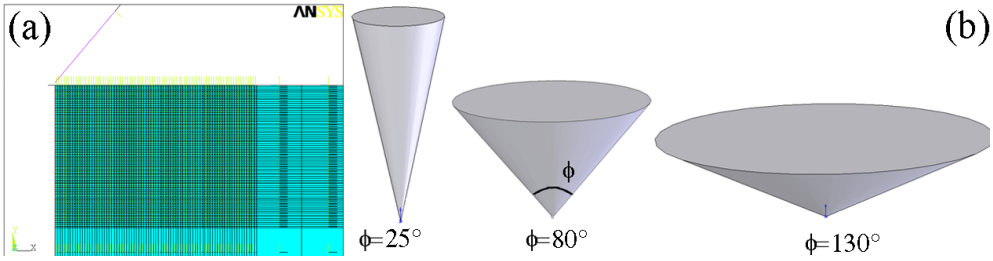

Figure 6. (a) Mesh distribution of the specimen model; (b) schematic diagram of the conical indenters with different corner angles.

Table 3. Elastic spring constant and deflection sensitivity of the probes.

Indenter	Spring constant (N m^{-1})	Deflection sensitivity (nm V^{-1})
Probe n°1	49.0	34.2
Probe n°2	35.2	34.5
Probe n°3	38.4	34.8

corresponding model the commercially available software ANSYS® (Ansys 8.1, Ansys inc.) has been used.

In this analysis we approach the numerical model as a non-linear contact problem. Both the indenter and the specimen are considered bodies of revolution and the pyramid indenter is approximated by an axisymmetric cone with the same equivalent corner angle. In this way it is possible to avoid a high computing time connected with the three-dimensional nature of the problem, with no introduction of considerable errors. Using a 3D pyramid indenter, in fact, there will be an elastic singularity at its edges, influencing the stress–strain response of only a tiny area close to these edges. In contrast, this will not affect the continuum plastic behaviour of the material with no interference in its load–deflection response [14].

In the present model it is assumed that the indenter is perfectly rigid and the test material is isotropic and homogeneous, elasto-plastic with isotropic hardening behaviour, obeying the von Mises yield criterion; the material was assumed to be elastic–fully plastic, thus with no strain hardening. This is an acceptable hypothesis, since the material is a polymer-based photoresist, which presents a perfectly plastic regime characterized by a constant yield stress [15].

As long as we simulate very small indentations, the meshed area near the indenter needs to be very fine in order to have a sufficient accuracy (figure 6(a)).

Once everything is defined (geometry, material and mesh) we are ready to simulate a typical indentation process moving the indenter with a downward–upward displacement (500 nm). This brings the indenter to push into the surface and then release, until it is free of contact with the specimen.

The indenter is modelled changing the corner angle (ϕ) with a step size of 10° angle, starting from a corner angle of 25° to 130° (figure 6(b)).

4. Theoretical model

Recently a general law has been proposed to the scientific community in order to compute the hardness as a function of size and shape of the indenter [16]. This law predicts how the material hardness depends on the geometry of the indenter and on the characteristics of the specimen

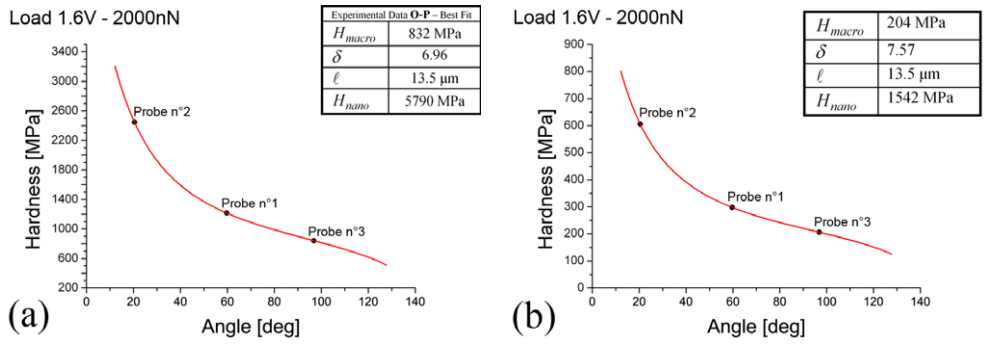

Figure 7. Experimental results for the three customized indentation probes and theoretical interpolation (red line): (a) data obtained with an OP approach; (b) data obtained with a direct measurement of the projected contact area.

material. In particular, considering a conical indenter with corner angle ϕ, the law predicts

$$H_{\text{cone}}(h,\phi) = H_{\text{macro}}\sqrt{1+\frac{\delta^2-1}{\delta^2 h/h^*(\phi)+1}} \tag{1}$$

where h is the depth of indentation, $\delta = H_{\text{nano}}/H_{\text{macro}}\ell$ the characteristic length, governing the transition from the nano- to the macro-scale, $h^*(\phi) = 3/2\ell(\tan^2((\pi-\phi)/2)(1/\sin((\pi-\phi)/2)) - 1/\tan((\pi-\phi)/2))H_{\text{cone}}$ the nominal hardness, H_{macro} the macro-hardness, and H_{nano} the nano-hardness. For $h/h^* \to 0$ or $\phi \to 0$, $H_{\text{cone}} \to H_{\text{nano}}$, whereas for $h/h^* \to \infty$ or $\phi \to \pi$, $H_{\text{cone}} \to H_{\text{macro}}$. Only for the case of $\delta \to \infty$ could equation (1) be simplified in this way:

$$H_{\text{cone}} = H_{\text{macro}}\sqrt{1+h^*/h} \tag{2}$$

as derived by Nix and Gao [2]. Note that the scaling law (2) was previously proposed by Carpinteri [17] for material strength (with h structural size).

In this paper we applied this theoretical approach, both to the experimental results and to the numerical data in order to find a continuous correlation between the indenter corner angle and the value of the measured material hardness. All these results are reported in the next section 5 in terms of experimental/numerical/theoretical comparison.

5. Results

The nanohardness was first calculated following the OP method [3–5], analysing the indentations performed during the experimental campaign. In this case the material is highly deformable in the plastic regime and a huge pile-up occurs. For this reason the hardness value will be extremely overestimated using the OP method. In some cases the material which piles up beside the indentation almost doubles the indentation depth. Thus means that the contact area should be four times bigger and the hardness value four times smaller than the OP values.

The hardness results obtained with this method are shown in figure 7(a).

One can see that these results are far away from the actual hardness of the material (∼200 MPa) and extremely overestimated. For this reason, since we are using standard tapping probes to indent the specimen, we also analysed the surface, imaging it in tapping mode. From the images, we were able to measure the projected contact area in a direct way and thus evaluate the hardness just by dividing the maximum load by this area.

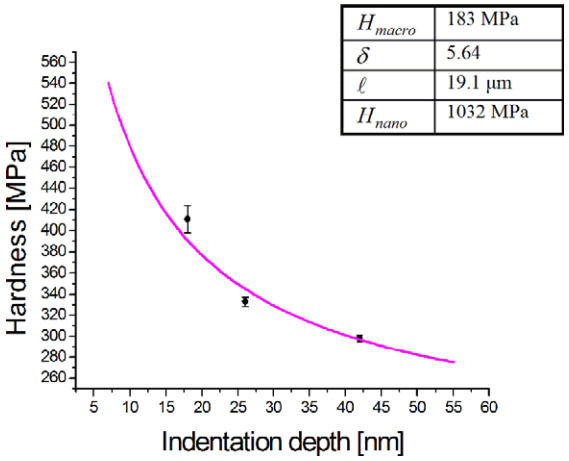

Figure 8. Experimental results of the measured hardness of the photoresist material, indenting at different applied loads and consequently at different indentation depths.

The hardness results obtained in this way are reported in figure 7(b). The huge difference between this results and the previous one appears evident. With a direct measurement of the contact area it is in fact possible to take into account the pile-up effect. In the insets the theoretical best-fit parameters are reported. The value of these parameters reveals again the high difference between the OP approach and the direct approach in the case of soft material. In the latter case the macro-hardness (H_{macro}) appears strictly close to the actual value of the polymer material while the nano-hardnes (H_{nano}), ∼7 times bigger than the macro-hardness, is ∼6 times smaller than the Young's modulus of the material. In addition, the characteristic length, found to be several microns, quantifies the size governing the transition from the nano- to the macro-scale. All these best-fit parameters are plausible and this confirms that the theoretical model is self-consistent.

As one can see in figure 5(a) the matrix of indentations is performed increasing the load from 0.4 to 1.6 V (∼500 to 2000 nN). So far the data reported refer only to the maximum load. Anyway the results in terms of hardness, related to the smaller loads, have been collected. We actually did not consider the 0.4 V (∼500 nN) load, because the indentation impression was too small to be distinguished from the roughness of the surface (in figure 5(b) it appears evident that in this case the material is practically not deformed and it is almost impossible to see the fourth column of indentations).

In figure 8 the results of the measured hardness versus applied load and consequently the indentation depth obtained with the functionalized indenter n°1 are reported. The behaviour is similar to the one observed by Nix and Gao in a previous work [2], with a measured hardness which increases on decreasing the indentation depth. It is interesting to underline that in this case the theoretical results in terms of best fit parameters are very close to those obtained changing the indenter shape (figure 7(b)). This means that these parameters depend only on the intrinsic properties of the material and not on the way of measuring them. This confirms again that the theoretical model is self-consistent.

As introduced in section 3, a FEM simulation has been performed. This numerical approach allowed us to verify the experimental results and to understand better how the indenter shape affects the hardness measurement. As a matter of fact, the study of the distribution of pressure in the contact area between the specimen and the indenter could provide much useful

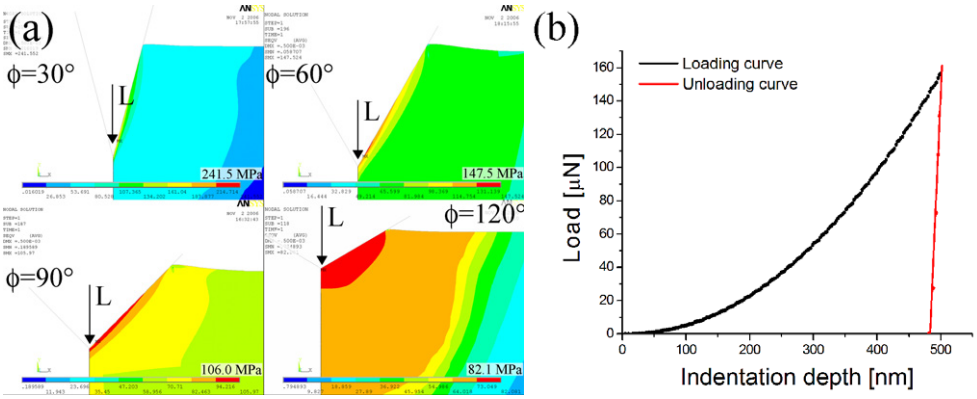

Figure 9. (a) Variation in the distribution of pressure in the indentation model increasing the corner angle of the conical indenter; L represents the applied load direction during the indentation process; (b) numerical load–displacement curve; the unloading part appears linear because of the elastic–fully plastic behaviour of the material.

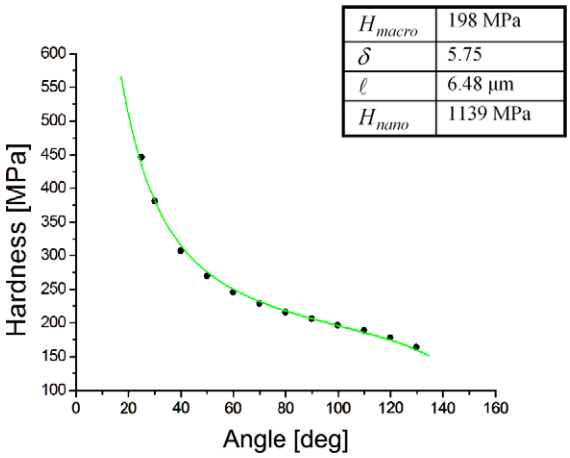

Figure 10. Numerical results for the indentation model over the whole range of the indenter corner angles and theoretical interpolation (green line).

information. In figure 9(a) four images of the numerical distribution of pressure corresponding to four different corner angles ($\phi = 30°$; $\phi = 60°$; $\phi = 90°$; $\phi = 120°$) are reported. It is evident that at small angles the contact pressure reaches very high values but actually concentrated at the very tip of the indenter. On the other hand, at big angles the pressure is more distributed over the whole contact region. This means that at small angles the specimen appears harder for the indenter to penetrate, since the regions far from the tip, but still in contact with the indenter, are not very stressed and thus not easily deformable. For this reason the hardness measurement reveals the trend reported in figure 10.

In figure 9(b) a numerical load–displacement curve is shown. This curve is related to the 90° corner angle indenter. As long as the material is considered to be elastic–fully plastic, the retract curve is linear, showing a fully elastic behaviour in the unloading phase.

In figure 10 the numerical hardness results are reported for the range of angles under study ($\phi = 25°-130°$). The hardness trend appears similar to that obtained experimentally, even if at

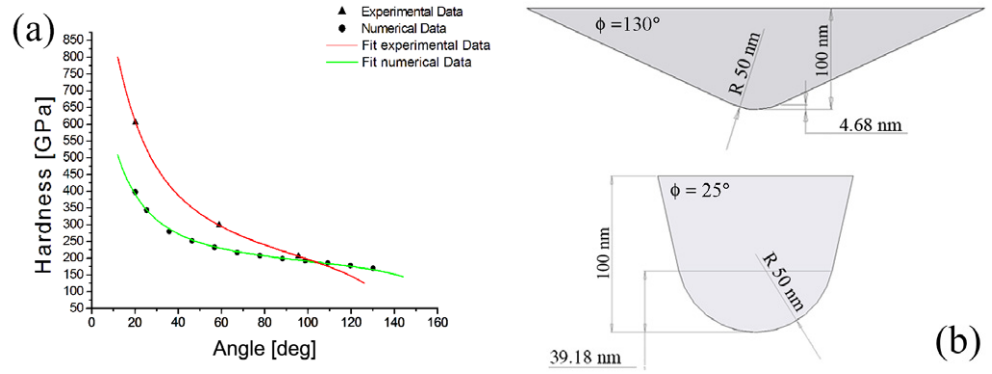

Figure 11. (a) Comparison between the experimental and numerical results, both interpolated using the 'general size/shape-effect law for nanoindentation'; (b) non-ideal indenters with different corner angles (130° upward and 25° downward) but with the same tip RoC (50 nm). For the first probe (130°) the indentation depth affected by the tip RoC is less than 5 nm; for the other probe (25°) the affected depth is almost ten times this (∼40 nm).

small angles an evident mismatch emerges in the results. Also the best fit parameters are very close to those obtained from the experimental data, showing an excellent agreement between numerical and experimental approach.

In figure 11(a) a direct comparison between the experimental and numerical results is reported. This comparison reveals a good agreement in the hardness behaviour even if an overestimation of the experimental results is evident at small angles. This is connected to the fact that the tip radius of curvature (RoC) of the real indenters is not negligible and affects the experimental results, making the measured hardness values bigger than the ideal one. The presence of a tip RoC in fact means that the indenter is not as sharp as it should be and for this reason it becomes more difficult to penetrate the substrate. At small angles this effect is more evident since the depth of the non-ideal part (the spherical part in figure 11(b)) is higher than at big angles. Work is in progress to treat such an effect.

6. Conclusion

Three different-shaped indentation probes have been designed and realized with a FIB machine. A whole experimental campaign has been performed with these indenters. A first Oliver–Pharr approach revealed a significant error in terms of values of measured hardness, due to the presence of a huge pile-up effect, which brings the method to significantly overestimate the results. A second approach, a direct measurement of the indented contact area, allowed us to consider the pile-up and to reduce the error. In this way, the results obtained in terms of hardness are comparable with the actual value of the material and quite close to those obtained by the FEM model. These results authorized us to deduce a theoretical relation which links the measured hardness value with the shape of the indenter. This relation follows a general scaling law for nanoindentation. Both the experimental and numerical results has been interpolated by this scaling law, with almost the same best-fit parameters.

The comparison between these three approaches reveals a good agreement in terms of IShE. By the way, a mismatch at small angles has been noticed. This is connected to the presence of a non-negligible tip RoC, which affects the experimental results and makes the measured hardness values slightly overestimated.

To correct this mismatch between the two approaches we are already trying to develop new numerical and theoretical models which take into account the tip radius of curvature.

Acknowledgments

The authors would like to acknowledge the FIB laboratory (a CNR-INFM-S3 laboratory), and especially Claudia Menozzi, for the collaboration in realizing the reshaped indentation probes.

This work has been supported by MIUR (PRIN 2004023199), Regione Emilia Romagna (LR no 7/2002, PRRIITT misura 3.1A) and Net-Lab SUP&RMAN (Hi-Mech District for Advanced Mechanics Regione Emilia Romagna).

References

[1] Doerner M F and Nix W D 1986 A method for interpreting the data from depth-sensing indentation instruments *J. Mater. Res.* **1** 601–9
[2] Nix W D and Gao H 1998 Indentation size effects in crystalline materials: a law for strain gradient plasticity *J. Mech. Phys. Solids* **46** 411–25
[3] Pharr G M, Oliver W C and Brotzen F R 1992 On the generality of the relationship among contact stiffness, contact area, and elstic modulus during indentation *J. Mater. Res.* **7** 613
[4] Oliver W C and Pharr G M 1992 An improved technique for determining hardness and elastic modulus using load and displacement sensing indentation experiments *J. Mater. Res.* **7** 1564
[5] Oliver W C and Pharr G M 2004 Measurement of hardness and elastic modulus by instrumented indentation: advances in understanding and refinements to methodology *J. Mater. Res.* **19** 1
[6] Li X and Bhushan B 2002 A review of nanoindentation continuous stiffness measurement technique and its applications *Mater. Charact.* **48** 11–36
[7] Saha R and Nix W D 2002 Effects of the substrate on the determination of thin film mechanical properties by nanoindentation *Acta Mater.* **50** 23–38
[8] Nix W D 1997 Elastic and plastic properties of thin films on substrates: nanoindentation techniques *Mater. Sci. Eng.* A **234–236** 37–44
[9] Bhushan B and Koinkar V N 1994 Nanoindentation hardness measurements using atomic force microscopy *Appl. Phys. Lett.* **64** 1653–5
[10] Bhushan B 2004 *Springer Handbook of Nanotechnology* (Berlin: Springer)
[11] Fischer-Cripps A C 2004 *Nanoindentation* (Berlin: Springer)
[12] Sader J E, Chon J W M and Mulvaney P 1999 Calibration of rectangular atomic force microscope cantilevers *Rev. Sci. Instrum.* **70** 3967–9
[13] Sader J E, Larson I, Mulvaney P and White L R 1995 Method for the calibration of atomic force microscope cantilevers *Rev. Sci. Instrum.* **66** 3789–98
[14] Bhattacharya A K and Nix W D 1988 Finite element simulation of indentation experiments *Int. J. Solids Struct.* **24** 881–91
[15] Yoshimoto K, Stoykovich M P, Cao H B, de Pablo J J, Nealey P F and Drugan W J 2004 A two-dimensional model of the deformation of photoresist structures using elastoplastic polymer properties *J. Appl. Phys.* **96** 1857–65
[16] Pugno N 2006 A general size/shape-effect law for nanoindentation *Acta Mater.* **55** 1947–53
[17] Carpinteri A 1994 Scaling laws and renormalization groups for strength and toughness of disordered materials *Int. J. Solids Struct.* **31** 291–302